Progress in Natural Science: Materials International 2012;22(6):572–584

Chinese Materials Research Society

Progress in Natural Science: Materials International

www.elsevier.com/locate/pnsmi
www.sciencedirect.com

REVIEW

Nanostructured $LiMn_2O_4$ and their composites as high-performance cathodes for lithium-ion batteries

Hui Xia[a,*], Zhentao Luo[b], Jianping Xie[b,]**

[a]*School of Materials Science and Engineering, Nanjing University of Science and Technology, Xiaolingwei 200, Nanjing 210094, China*
[b]*Department of Chemical and Biomolecular Engineering, National University of Singapore, 9 Engineering Drive 1, Singapore 117576, Singapore*

Received 30 July 2012; accepted 7 October 2012
Available online 29 December 2012

KEYWORDS

Lithium manganese oxide;
Cathode;
Lithium-ion batteries;
Nanostructure;
Nanocomposite

Abstract Improvement of the energy density and power density of the lithium-ion batteries is urgently required with the rapid development of electric vehicles and portable electronic devices. The spinel $LiMn_2O_4$ is one of the most promising cathode materials due to its low cost, nontoxicity, and improved safety compared with commercial $LiCoO_2$. Developing nanostructured electrode materials represents one of the most attractive strategies to dramatically enhance battery performance, such as capacity, rate capability and cycling life. Currently, extensive efforts have been devoted to developing nanostructured $LiMn_2O_4$ and $LiMn_2O_4$/carbon nanocomposites to further improve the rate capability of lithium-ion batteries for high-power applications. In this paper, recent progress in developing nanostructured $LiMn_2O_4$ and $LiMn_2O_4$/carbon nanocomposites is reviewed, and the benefits to the electrochemical performance of $LiMn_2O_4$-based cathodes by using these electrode materials are also discussed.

*Corresponding author. Tel.: +86 25 84315606; fax: +86 25 84315159.
**Corresponding author. Tel.: +65 65161067; fax: +65 67791936.
E-mail addresses: xiahui@njust.edu.cn (H. Xia), chexiej@nus.edu.sg (J. Xie).

Peer review under responsibility of Chinese Materials Research Society.

ELSEVIER Production and hosting by Elsevier

1. Introduction

Due to the fast depletion of fossil fuels and the associated environmental problems, there has been a strong and ever-increasing demand for renewable energy and reliable devices for energy conversion and storage. Lithium-ion batteries, with their superior energy density, have become attractive energy-storage systems for portable electronic devices, such as cell phones, digital cameras and laptops. Currently, the worldwide market for lithium-ion batteries is valued as 10 billion dollars

1002-0071
http://dx.doi.org/10.1016/j.pnsc.2012.11.014

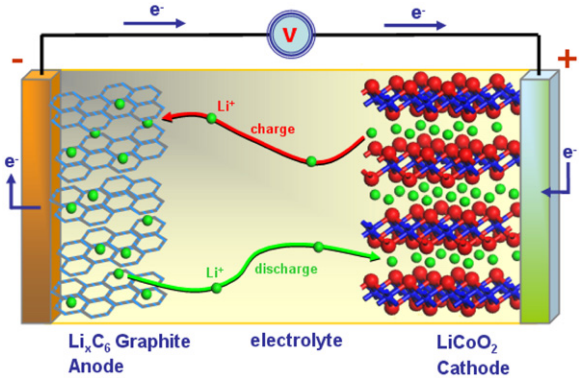

Fig. 1 Schematic illustration of a lithium-ion battery. The anode (graphite) and the cathode ($LiCoO_2$) are separated by a non-aqueous liquid electrolyte. Reprinted from Ref. [1] with permission by John Wiley and Sons.

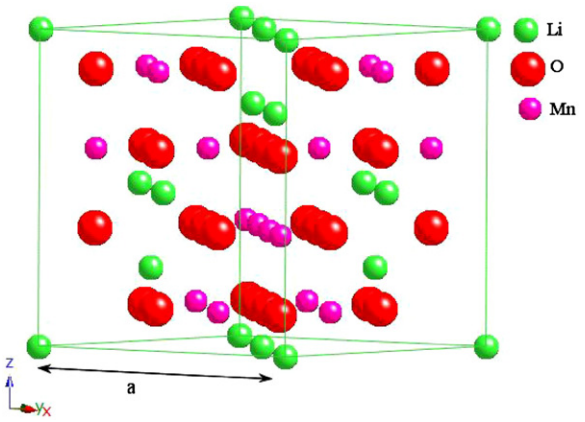

Fig. 2 The crystal structure of spinel $LiMn_2O_4$.

per annum and is still expanding. The emerging new technologies, such as electric vehicles for transportation and smart grids for utilizing renewable energy sources, will largely depend on the development and application of lithium-ion batteries for large-scale energy storage [1–4].

In lithium-ion batteries, lithium ions are shuttled between the two insertion host electrodes (cathode and anode) during the charge/discharge processes. Fig. 1 illustrates a typical lithium-ion battery, which consists of a graphite negative electrode (anode), a non-aqueous liquid electrolyte, and a positive electrode (cathode) formed by layered $LiCoO_2$. During the charging process, lithium ions are extracted from $LiCoO_2$, pass across the electrolyte, and are inserted into the graphene layers of the graphite. The discharge is the reverse process in which lithium ions are de-intercalated from the graphite and re-inserted into the $LiCoO_2$ cathode. In the meantime, electrons pass through the external circuit for charge compensation. In commercial lithium-ion batteries, graphite is used as the anode while lithium transition metal oxides, such as $LiCoO_2$, $LiFePO_4$, and $LiMn_2O_4$, are employed as the cathode [5–7].

For the cathode materials, each system has its own advantages and disadvantages. The layered $LiCoO_2$ has revolutionized portable electronics like cell phones and laptops, but the high cost, toxicity, and safety concerns prevented $LiCoO_2$ from being used in large-scale batteries and transportation [8,9]. Although $LiFePO_4$ has improved safety, the high cost of producing carbon-coated nano-$LiFePO_4$ limits its application in large-scale batteries [10]. In contrast, spinel $LiMn_2O_4$ has become the most attractive cathode material for transportation and large-scale batteries due to its low cost, environmental friendliness, good structural stability, and much improved safety [11].

As illustrated in Fig. 2, $LiMn_2O_4$ adopts the spinel structure with space group $Fd\bar{3}m$ in which the Li and Mn occupy the 8a tetrahedral and 16d octahedral sites of the cubic close-packed oxygen ions, respectively. The edge-shared octahedral Mn_2O_4 host structure is highly stable and possesses a series of intersecting tunnels formed by the face-sharing of tetrahedral lithium (8a) sites and empty octahedral (16c) sites. Such tunnels allow the three-dimensional diffusion of lithium. The lithium intercalation/deintercalation into/from the 8a tetrahedral sites occurs at about 4 V with the maintaining of the initial cubic spinel symmetry. Surplus lithium can be intercalated into the spinel $LiMn_2O_4$ to reach a maximum composition of $Li_2Mn_2O_4$, which occurs at about 3 V against the lithium anode with a phase transformation from cubic to tetragonal phase. The cubic to tetragonal phase transition, often referred to as Jahn–Teller distortion, is accompanied by a 6.5% increase in the unit cell volume, which damages the structural integrity of the electrode during charge/discharge cycling and results in rapid capacity fading [12]. To prevent Jahn–Teller distortion, $LiMn_2O_4$ are only used below 4 V vs. Li/Li^+ with a limited practical capacity of around 140 mA h/g (the theoretical capacity of $LiMn_2O_4$ is 148 mA h/g while the theoretical capacity of $Li_2Mn_2O_4$ is 296 mA h/g). However, $LiMn_2O_4$ tends to exhibit capacity fading even in the 4 V region, especially at elevated temperatures. Several detrimental effects, including Jahn–Teller distortion at the surface of the particles under conditions of nonequilibrium cycling [13], dissolution of Mn into the electrolyte [14], formation of two cubic phases in the 4 V region [15], loss of crystallinity [16], and development of micro-strain [17] during cycling, could be the source of the capacity fading. These major detrimental effects are summarized in Table 1. Several strategies have been developed to overcome the detrimental effects (Table 1), such as the over-oxidation of Mn that leads to the formation nonstoichiometric $LiMn_2O_{4+\delta}$, the cationic substitutions that results in $LiM_yMn_{2-y}O_4$ (M = Li, Cr, Co, Ni, and Cu) and the surface modification. However, these strategies usually cause decrease in capacity. On the other hand, the reduction of particle size is a promising strategy since it can alleviate these detrimental effects (except for the case of dissolution of Mn) and also improve the electrochemical performance of $LiMn_2O_4$.

Although lithium-ion batteries can provide higher energy density than other secondary battery systems, their power density remains too low for high power applications [e.g., electric vehicle (EV)]. The power density of lithium-ion batteries is limited by the low rate capability of the electrode materials. In particular, the slow lithium ion and electron diffusion in the cathode materials lead to insufficient lithium ion insertion/extraction under high charge/discharge rates [18]. Two methods are generally employed to increase the rate capability of the cathode materials. One method is to reduce the crystallite size and particle size of the cathode materials from micrometer to nanometer so that the electron and lithium ion diffusion paths can be shortened [19]. Another method is to add conductive additives to the cathode materials to improve their electrical conductivity [20]. It was found that

Table 1 Detrimental effects that induce instability and capacity fading of $LiMn_2O_4$.

Detrimental effect	Mechanism of the detrimental effect	General solution	Limitation of current solution	Prospect on how to improve
Jahn–Teller distortion	Severe volume change	Nonstoichiometric spinel, metal ion doping	Low capacity	Reduce particle size
Dissolution of Mn	Disproportionation reaction	Surface modification	Low capacity	Reduce coating materials
Formation of two cubic phases	Structure instability	Nonstoichiometric spinel	Low capacity	Reduce particle size
Loss of crystallinity	Structure degradation	Nonstoichiometric spinel	Low capacity	Reduce particle size
Development of micro-strain	Volume change	Metal ion doping	Low capacity	Reduce particle size

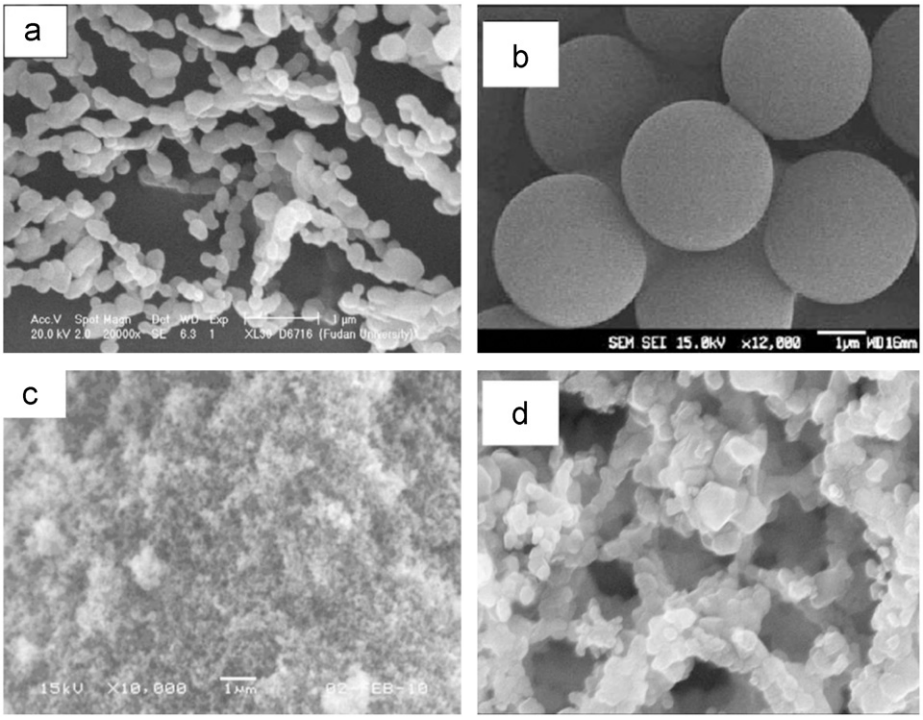

Fig. 3 SEM images of $LiMn_2O_4$ nanoparticles synthesized by (a) nstarch-assisted sol–gel method (reprinted from Ref. [45] with permission from Elsevier), (b) ultrasonic spray pyrolysis (reprinted from Ref. [36] with permission from Elsevier), (c) flame spray pyrolysis (reprinted from Ref. [42] with permission from Elsevier), and (d) a resorcinol–formaldehyde route (reprinted from Ref. [44] with permission from Elsevier).

by using nanostructured $LiMn_2O_4$ and $LiMn_2O_4$/carbon nanocomposites, the rate capability, the structural stability of $LiMn_2O_4$, and the cycling stability could all be improved [21]. To date, various nanostructures of $LiMn_2O_4$ (e.g., nanoparticles [22], nanorods [21,23], nanowires [24,25], and nanotubes [26,27]) and various $LiMn_2O_4$/carbon nanocomposites (e.g., carbon coated $LiMn_2O_4$ [28], $LiMn_2O_4$/carbon nanotube [29,30], and $LiMn_2O_4$/graphene nanocomposites [31]) have been developed and applied as the cathode materials. In this review, we will discuss the recent progress in developing nanostructured $LiMn_2O_4$ and $LiMn_2O_4$/carbon nanocomposites and the benefits to the electrochemical performance of $LiMn_2O_4$-based cathodes by utilizing these electrode materials.

2. Nanostructured $LiMn_2O_4$

2.1. *$LiMn_2O_4$ nanoparticles*

$LiMn_2O_4$ is conventionally prepared by the solid-state reaction between lithium and manganese salts. However, these preparations suffer from problems such as inhomogeneity, irregular morphology, large particle size, poor control of stoichiometry and long period of calcination. Recently, many wet chemical methods including sol–gel, pechini, combustion, precipitation, spray pyrolysis and hydrothermal synthesis have been employed to synthesize $LiMn_2O_4$ [32–39]. In contrast to the solid-state methods, the wet chemical methods have better control of stoichiometry, require lower calcination temperature and relatively

shorter processing time, and can produce nano-sized particles with a narrow size distribution. However, for the wet chemical methods, hard aggregation between the nanoparticles could occur during the post-calcining process. In addition, the calcining temperature needs to be optimized to obtain organic free, phase pure crystalline powders since high specific capacity and good rate capability can only be obtained from $LiMn_2O_4$ nanoparticles with a high degree of crystallinity [18]. $LiMn_2O_4$ nanoparticles with poor crystallinity have excessive amount of surface defects that can adversely affect electrochemical properties of the nanoparticles [29]. More importantly, the spinel structure may not be perfectly constructed in the poorly crystallized $LiMn_2O_4$ so that not all lithium ions can be reversibly extracted and inserted. Therefore, when using these wet chemical methods to prepare $LiMn_2O_4$ nanoparticles, caution must be taken to obtain nano-sized particles with high crystallinity.

Various chelating agents, such as citric acid, fumaric acid and starch, have been used to assist the sol–gel synthesis of $LiMn_2O_4$ nanoparticles [34,40,41]. Recently, Tang et al. [41] synthesized nanochain-structured $LiMn_2O_4$ by a starch-assisted sol–gel method. $LiMn_2O_4$ prepared by this method displayed a nanochain shape that consisted of nanobeads of about 100 nm in diameter (Fig. 3a). The nanochain-structured $LiMn_2O_4$ demonstrated better rate capability and cycling stability than the commercial $LiMn_2O_4$ composed of aggregated submicron-sized particles. The authors attributed the superior electrochemical performance of the nanochain-structured $LiMn_2O_4$ to its interconnected nanocrystalline morphology, which may facilitate lithium ion transport and allow good rate performance [41].

Spray pyrolysis is another widely used method that can continuously produce hypercomplex and uniform particles by spray-pyrolizing the solution mixture of reagents. Spherical $LiMn_2O_4$ composed of 10 nm-sized primary nanoparticles was synthesized by an ultrasonic spray pyrolysis method (Fig. 3b) [36]. It is interesting to note that these $LiMn_2O_4$ nanoparticles did not show capacity fading in the 3 V region even after 50 cycles. The primary crystalline nanoparticles still suffered the Jahn–Teller distortion; however, the strain within the particles induced the phase transition to occur in random directions, which allowed the nanoparticles to sustain the volume change. Yi et al. prepared $LiMn_2O_4$ cathode powders comprising nanoparticles by flame spray pyrolysis using an aqueous spray solution prepared from inexpensive metal salts [42]. The $LiMn_2O_4$ powders had non-aggregation characteristics as shown in Fig. 3c, which indicated that flame spray pyrolysis could be a promising method to prepare $LiMn_2O_4$ nanoparticles without severe particle aggregation.

The best electrochemical performance of $LiMn_2O_4$ nanoparticles was reported by Shaju and Bruce [43]. They synthesized stoichiometric $LiMn_2O_4$ by a one-pot resorcinol–formaldehyde route. Similar results have been reported by Chen et al. using a modified resorcinol–formaldehyde route [44]. As shown in Fig. 3d, the interconnected $LiMn_2O_4$ nanoparticles with diameters of 50 to 100 nm formed a porous structure. This nanocrystalline $LiMn_2O_4$ demonstrated a high initial capacity of 131 mA h/g and retained 118 mA h/g after 200 cycles at a discharge rate of C/2. It also exhibited excellent rate capability (Fig. 4), retaining 90% of its capacity at 40 C and 85% at 60 C. The cycling stability of this material was greatly improved as compared to the conventionally synthesized bulk $LiMn_2O_4$ or nanoparticle $LiMn_2O_4$ synthesized by a different sol–gel route, which indicated that the nanocrystalline $LiMn_2O_4$ prepared

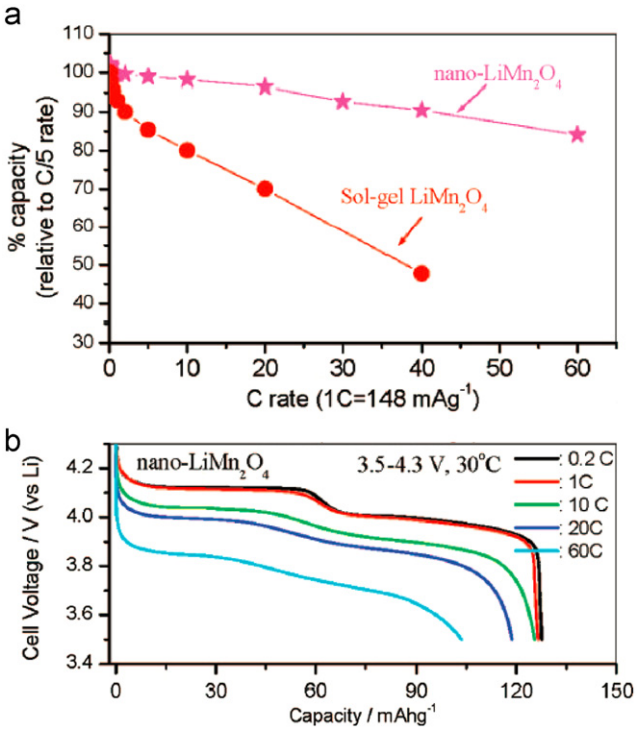

Fig. 4 (a) Comparison of rate performance between nano-$LiMn_2O_4$ prepared by resorcinol–formaldehyde route and the sol–gel prepared $LiMn_2O_4$. (b) The discharge voltage profiles of nano-$LiMn_2O_4$ at different discharge rates. Reprinted from Ref. [43] with permission from American Chemical Society.

using the resorcinol–formaldehyde route might possess a stabilized surface that inhibits Mn dissolution [43].

The $LiMn_2O_4$ nanoparticles synthesized by wet chemical methods typically need a high-temperature calcination process to form the spinel structure. Recently, hydrothermal method has been demonstrated as an attractive low-temperature route to prepare crystalline $LiMn_2O_4$ [46–48]. However, the previously proposed hydrothermal synthesis procedures have some disadvantages. For examples, multiple reagents including oxidants (e.g., H_2O_2), reductants (e.g., glucose), or low-valence Mn sources [e.g., $Mn(NO_3)_2$] were used together with the manganese sources to obtain mixed valences of Mn^{4+} and Mn^{3+} in the starting materials, which added considerable complexity to the synthesis. Jiang et al. [46] synthesized $LiMn_2O_4$ nanoparticles hydrothermally at 200 °C directly from γ-MnO_2 and aqueous solution of LiOH without any additional reagents. It was found that 3 days of hydrothermal reaction could produce highly crystallized $LiMn_2O_4$ nanoparticles (30–50 nm, Fig. 5a) with good electrochemical performance. In another study, $LiMn_2O_4$ nanoparticles (50–300 nm, Fig. 5b) were hydrothermally synthesized from MnO_2, $Mn(NO_3)_2$, and aqueous solution of $LiOH \cdot H_2O$ at 280 °C for 36 h [47]. The distinctive well-defined crystal faces indicate that the nanoparticles are single spinel crystals of octahedral shape with well-developed {1 1 1} planes. Later, Okubo et al. [18] synthesized nanocrystalline $LiMn_2O_4$ by a hydrothermal reaction of nano-sized orthorhombic $LiMnO_2$, LiOH, and H_2O (Fig. 5c). The crystallite size of the nanocrystalline $LiMn_2O_4$ (15–210 nm) was controlled by varying the amount LiOH, temperature and reaction time. In general, Jahn–Teller

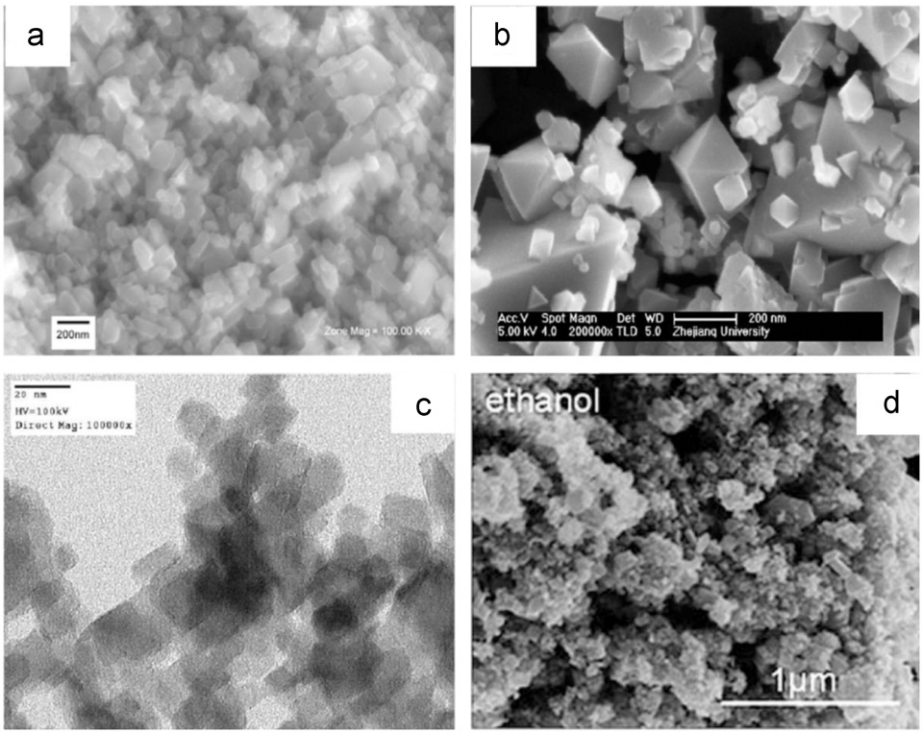

Fig. 5 SEM and TEM images of $LiMn_2O_4$ nanoparticles prepared using different hydrothermal methods by (a) Jiang (reprinted from Ref. [46] with permission from Elsevier), (b) Wu (reprinted from Ref. [47] with permission from Elsevier), (c) Okubo (reprinted from Ref. [18] with permission from American Chemical Society), and (d) Liddle (reprinted from Ref. [48] with permission from Royal Society of Chemistry).

distortion from cubic spinel to tetragonal spinel is accompanied by a large unit cell expansion, and the lithium ion intercalation proceeds by fractional change of the two phases. When crystallite size is considerably large, full lithiation throughout the particle cannot be achieved due to the slow movement of the domain boundaries. In this study, it was found that when crystallite size was sufficiently small (~15 nm), the nanocrystals could not accommodate domain boundaries between Li-rich and Li-poor phases due to interface energy, and the lithiation would proceed via solid solution state without domain boundaries, which allowed fast Li-ion insertion during entire discharge process [18]. Liddle et al. synthesized $LiMn_2O_4$ nanoparticles through a very simple and fast hydrothermal process in which $KMnO_4$ reacted with organic reductants (e.g., alcohols and acetone) and the aqueous solution of LiOH [48]. The spinel $LiMn_2O_4$ phase with no other impurities was formed after a short reaction time (~5 h) at a relatively low temperature (180 °C). Fig. 5d shows the synthesized $LiMn_2O_4$ that was composed of nanoparticles with sizes between 10 and 30 nm as majority and some larger particles (100–300 nm). However, severe nanoparticle aggregation and oxygen deficiency were observed in the as-prepared samples [49]. Promising electrochemical behavior of these $LiMn_2O_4$ nanoparticles could only be achieved after annealing in oxygen at 500 °C to remove the oxygen deficiency.

2.2. One-dimensional (1-D), two-dimensional (2-D) and three-dimensional (3-D) $LiMn_2O_4$ nanostructures

In addition to the $LiMn_2O_4$ nanoparticles, extensive efforts have also been devoted to developing other $LiMn_2O_4$ nanostructures. 1-D nanostructures, such as nanorods, nanowires and nanotubes, are particularly attractive because they have large surface-to-volume ratio that allows for efficient active material–electrolyte contact and can also provide efficient 1-D electron transport pathways and facile strain relaxation during battery charge and discharge [50]. Moreover, the nonwoven fabric morphology constructed by these 1-D nanostructures can suppress the aggregation and grain growth at high temperature, and the potential barrier between the nano-sized grains can be ignored [24]. However, the reported single crystalline 1-D nanostructures are generally metal oxides with an anisotropic crystal structure because the materials with a cubic spinel crystal structure (e.g., $LiMn_2O_4$) cannot easily grow in the one-dimensional direction. Therefore, most of the recent works used 1-D MnO_2 nanostructures as a self-template to prepare 1-D $LiMn_2O_4$ nanostructures.

Kim et al. [50] reported the hydrothermal synthesis of single-crystalline β-MnO_2 nanorods and their conversion into free-standing single-crystalline $LiMn_2O_4$ nanorods in a simple solid-state reaction. The $LiMn_2O_4$ nanorods, having an average diameter of 130 nm and length of 1.2 μm (Fig. 6a), could deliver 100 mA h/g at a current density of 148 mA/g (1 C). Hosono et al. [24] synthesized high-quality single crystalline $LiMn_2O_4$ nanowires by using $Na_{0.44}MnO_2$ nanowires as a self-template. The sodium/lithium ion exchange and the addition of more lithium were performed in molten salts of $LiNO_3$ (88 mol%) and LiCl (12 mol%) at 450 °C for 1 h. This molten salt process produced a mixture of $Li_{0.44}MnO_2$ and Li_2MnO_3, which was finally converted to $LiMn_2O_4$ when heated at 800 °C for 1 h. The nanowire morphology of $Na_{0.44}MnO_2$ was well maintained, and $LiMn_2O_4$ nanowires

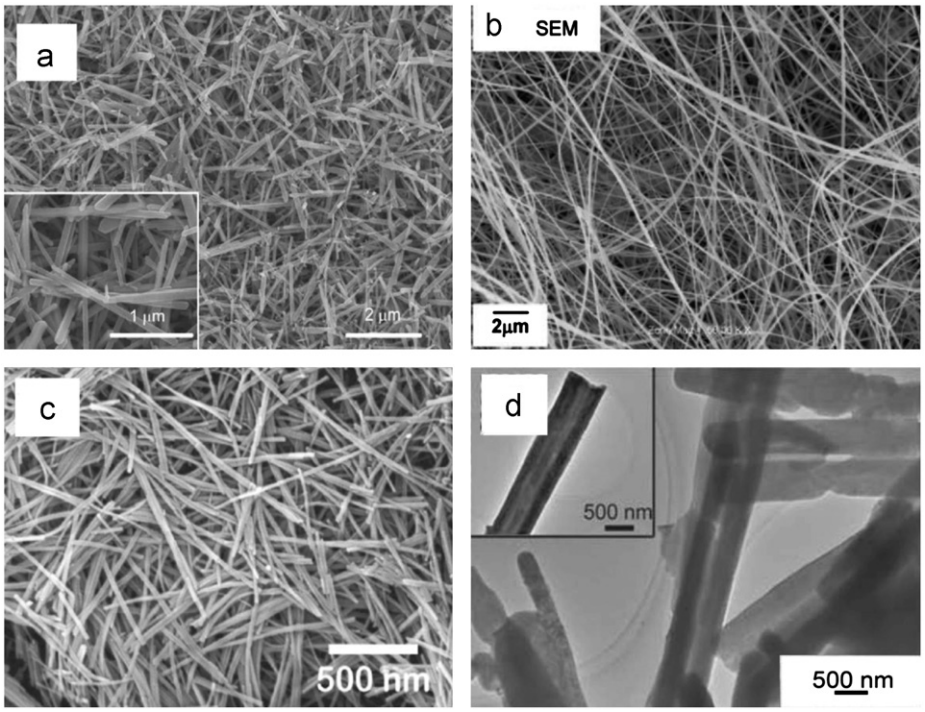

Fig. 6 (a) SEM image of $LiMn_2O_4$ nanorods synthesized from β-MnO_2 nanorods. Reprinted from Ref. [50] with permission from American Chemical Society. (b) SEM image of $LiMn_2O_4$ nanowire synthesized from $Na_{0.44}MnO_2$ nanowires. Reprinted from Ref. [24] with permission from American Chemical Society. (c) SEM image of $LiMn_2O_4$ nanowires synthesized from α-MnO_2 nanowires. Reprinted from Ref. [51] with permission from American Chemical Society. (d) TEM image of $LiMn_2O_4$ nanotubes synthesized from β-MnO_2 nanotubes. Reprinted from Ref. [26] with permission from John Wiley and Sons.

with the diameters of 50–100 nm were obtained (Fig. 6b). By employing a different self-template α-MnO_2 nanowires, Lee et al. successfully synthesized single crystalline $LiMn_2O_4$ nanowires with diameters less than 10 nm (Fig. 6c) using a solid-state reaction [51]. The $LiMn_2O_4$ nanowire electrode exhibited excellent rate capability and cycling stability as shown in Fig. 7. The average discharge capacity of the $LiMn_2O_4$ nanowire electrode at the current rate of 10 C was around 105 mA h/g, and those at 60 C and 150 C were around 100 and 78 mA h/g, respectively. These large capacities at high current rates arise from the nanowire morphology and the high quality of the single crystal, which can shorten the diffusion lengths of both the lithium and electrons. Single crystalline $LiMn_2O_4$ nanotubes with an average diameter of about 600 nm, a wall thickness of about 200 nm and a length of 1–4 μm have also been synthesized using MnO_2 nanotubes as a self-template (Fig. 6d) [26]. However, due to the large dimensions in diameter and wall thickness, the $LiMn_2O_4$ nanotubes do not exhibit superior cycling stability and rate capability compared to the $LiMn_2O_4$ nanowires.

Two-dimensional nanostructures, such as nanosheets, can also be beneficial for fast lithium ion transport. Specifically, 2-D SnO_2 nanosheet anodes were reported to have faster lithium ion diffusion kinetics and superior high-rate capability owing to their 2-D geometry [52]. Like 1-D nanostructures, since the cubic spinel $LiMn_2O_4$ cannot easily grow in 2-D direction, MnO_2 nanosheets, which can be easily prepared, could be used as a self-template for preparing $LiMn_2O_4$ nanosheets [53]. Sun et al. reported the synthesis of nanoporous $LiMn_2O_4$ nanosheets using MnO_2 nanosheets as a template [54]. The preparation process is shown in Fig. 8a. Ultrathin MnO_2 nanosheets were synthesized by a redox reaction of $HMnO_4$. After that, the MnO_2 nanosheets were added into the solution of diethyl ether and lithium methide to form LiOH-coated MnO_2 nanosheets. The resultant solid powder was transferred to a furnace and annealed at 700 °C for 4 h in a nitrogen atmosphere, forming the porous single crystalline $LiMn_2O_4$ nanosheets. The SEM image (Fig. 8b) shows that each nanostructured sheet is composed of small $LiMn_2O_4$ nanoparticles. Fig. 8c shows a comparison of rate capability between porous $LiMn_2O_4$ nanosheets (PS-$LiMn_2O_4$) and $LiMn_2O_4$ powders produced by solid-state reaction (SS-$LiMn_2O_4$). It is clear that the discharge capacities of PS-$LiMn_2O_4$ are much higher than that of SS-$LiMn_2O_4$. The superior electrochemical performance of PS-$LiMn_2O_4$ was attributed to the nanoporous structure, the high crystallinity and the exposed {1 1 1} facets that improved the structural stability [54].

Three-dimensional porous nanostructures with large surface area could exhibit higher durability in the lithium insertion/extraction process at a high current density, owing to the short lithium ion diffusion lengths in the 3-D channels of the electrode [55–57]. Xi et al. synthesized porous $LiMn_2O_4$ microspheres by a solid-state reaction using α-MnO_2 urchin-like structures as a self-template [58]. As shown in Fig. 9a, the $LiMn_2O_4$ microspheres with an average diameter of about 2 μm are composed of nanoparticles less than 100 nm. A similar porous structure of $LiMn_2O_4$ formed by using $MnCO_3$ as the self-template was reported by Uchiyama et al. [59]. The macroscopic morphologies of $MnCO_3$ can be tuned between spherical and rhombohedral shapes using different agar contents. Using the biomimetic nanostructures of $MnCO_3$ prepared in agar matrix, a highly porous network

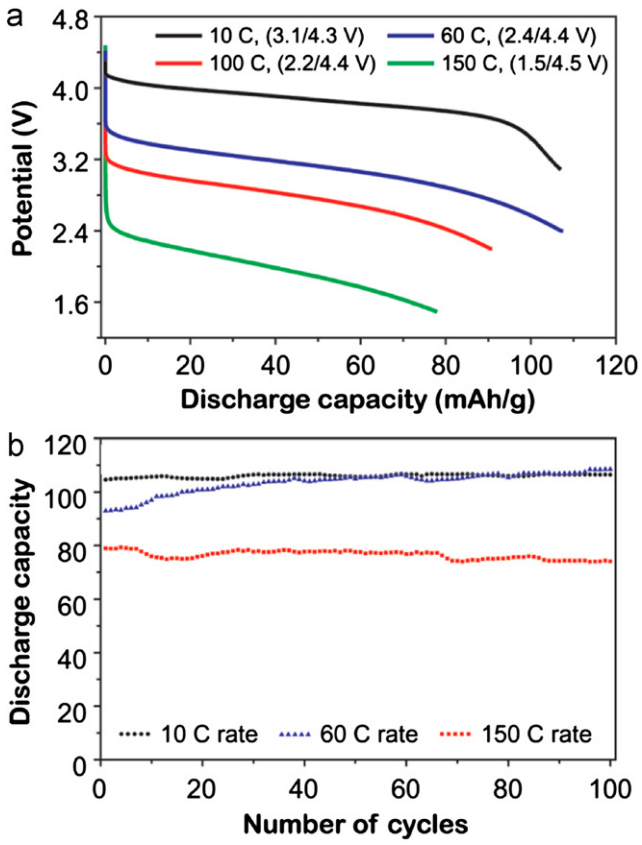

Fig. 7 (a) Discharge curves of the $LiMn_2O_4$ nanowires at different rates after charging at 1 C. (b) Discharge capacity as a function of cycle number for the $LiMn_2O_4$ nanowire electrode cycled at different current rates. Reprinted from Ref. [51] with permission from American Chemical Society.

consisting of $LiMn_2O_4$ nanoparticles of 50–200 nm in diameter (Fig. 9b) was obtained with high durability for lithium charge/discharge cycles at a high current density. It was found that $MnCO_3$ could be partially converted into MnO_2 when heated at 290 °C for 2 h in air [60]. After performing a chemical etching with HCl, the $MnO_2/MnCO_3$ mixture could be converted into a hollow MnO_2 structure. Wu et al. used the hollow MnO_2 microcubes as templates and successfully synthesized hollow porous $LiMn_2O_4$ microcubes (Fig. 9c) [60]. The hollow porous $LiMn_2O_4$ microcubes demonstrated superior lithium-storage capacity with a stable cycle life and a good rate capability compared to the solid-state reaction synthesized $LiMn_2O_4$. For the 3-D porous $LiMn_2O_4$ nanosturctures, it is difficult to control the particle size and pore size distributions. Jiao et al. first reported the synthesis of ordered mesoporous $LiMn_2O_4$ [61]. In their synthesis procedure, the 3-D mesoporous Mn_2O_3 synthesized using mesoporous silica as the template was converted to Mn_3O_4 and finally to 3-D mesoporous $LiMn_2O_4$ by a solid-state reaction with LiOH (Fig. 9d). Despite having a high surface area of 90 m^2/g, the mesoporous $LiMn_2O_4$ could achieve higher rate capability than that of the corresponding bulk material (50% higher capacity at a rate of 30 C) at ambient temperature and good stability at elevated temperatures, without the need for the deliberate coating or doping with foreign ions.

Luo et al. synthesized $LiMn_2O_4$ nanorods, nanothorn microspheres and hollow nanospheres by using corresponding MnO_2 nanostructures as templates [62]. The surface morphologies of these $LiMn_2O_4$ nanostructures are shown in Fig. 10a–c. Their electrochemical lithium insertion/extraction properties were extensively investigated. Fig. 10d shows the cycle performance of the three $LiMn_2O_4$ nanostructures between 3 and 4.3 V at 1 C rate. The $LiMn_2O_4$ hollow nanospheres exhibit the best cycle performance and rate capability among the three nanostructures. Compared to the 1-D nanorods or 3-D nanothorn microspheres, the 3-D hollow nanospheres could provide larger interface area between the electrode material and the electrolyte, smaller particle size and more inter-space that could facilitate fast lithium ion transport and alleviate the volume expansion of the electrode during charge/discharge [63].

2.3. $LiMn_2O_4$/carbon nanocomposites

The small dimensions of nano-sized active materials can greatly increase the electrode–electrolyte contact area, facilitate charge-transfer and diffusion kinetics during Li insertion/extraction, and offer improved tolerance to structural distortion. Hence, these nanomaterials are promising to achieve attractive power capability and cycling stability. However, severe aggregation of nanoparticles commonly occurs during electrode preparation and charge/discharge cycling. The aggregation can reduce the accessible interface area between electrode and electrolyte. Moreover, electrolyte decomposition may induce the dissociation of individual nanoparticles or agglomerates from the electrode, resulting in an irreversible loss of capacity and electrode integrity. As a semiconductor material, $LiMn_2O_4$ also suffers from its low electrical conductivity. Therefore, $LiMn_2O_4$ nanoparticles alone with low electrical conductivity and a tendency to aggregate cannot achieve great improvement in rate capability and cycling stability. To solve these problems, carbon materials [e.g., carbon nanotubes (CNT) and graphene nanosheets (GNS)] with high electrical conductivity, chemical stability and mechanical robustness have been added into $LiMn_2O_4$ to make $LiMn_2O_4$/carbon nanocomposites [28,29,64–68]. These carbon materials can provide excellent conducting support for the $LiMn_2O_4$ electrode, suppress aggregation of nanoparticles, and minimize structural degradation due to volume changes induced by lithium insertion/extraction. However, the introduction of carbon into $LiMn_2O_4$ may increase the oxygen deficiency at the surface of $LiMn_2O_4$ and cause detrimetnal effects. Therefore, low-temperature and short-time processing at high temperature are usually employed for synthesizing $LiMn_2O_4$/carbon composites to prevent the reaction between $LiMn_2O_4$ and carbon.

The preparation of carbon-composite-based cathode materials is still a challenge, especially for lithium transition metal compounds that requirie high-temperature solid-state syntheses. Yue et al. synthesized the $LiMn_2O_4$/carbon (C) composite (7.79 wt% carbon content) by a hydrothermal method [64]. The particles of the $LiMn_2O_4$/C composite were in the size range between 200 and 400 nm. The hydrothermally synthesized $LiMn_2O_4$/C composite exhibited improved rate capability compared to the ball mill prepared $LiMn_2O_4$/C composite because the former has higher electrical conductivity due to the better $LiMn_2O_4$–C contact. To obtain $LiMn_2O_4$/C composite with smaller particle sizes, Patey and Novak et al. synthesized

$LiMn_2O_4$/C nanocomposites using a flame spray pyrolysis (FSP) method [28]. The authors developed a strategy to combine

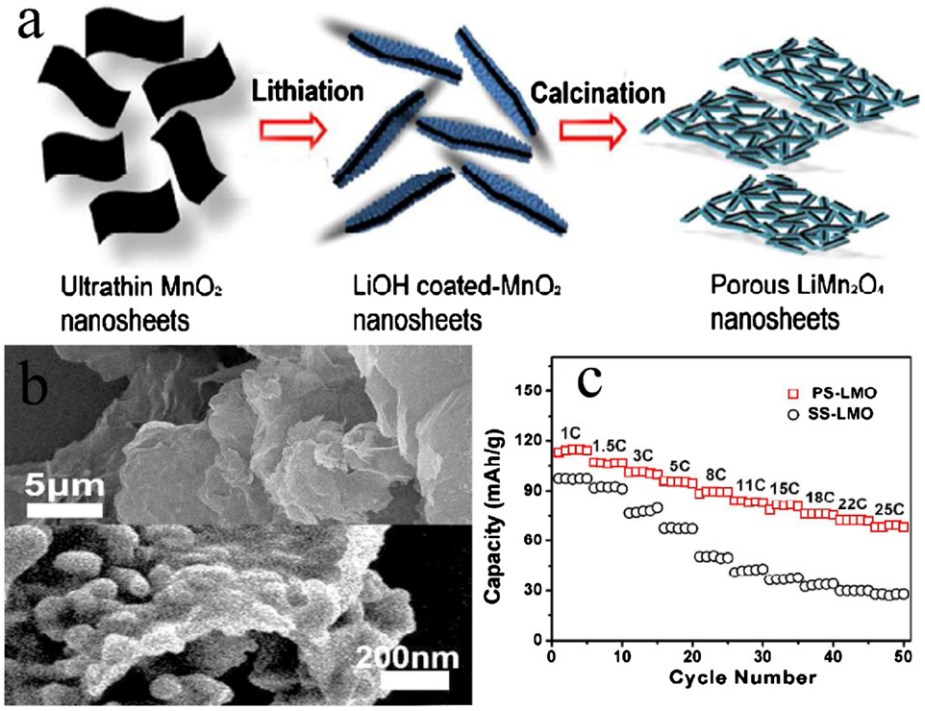

Fig. 8 (a) Schematic representation of the *in-situ* conversion of ultrathin MnO_2 nanosheets to porous $LiMn_2O_4$ nanosheets. (b) SEM images of the porous $LiMn_2O_4$ nanosheets. (c) Variation in discharge capacities *versus* cycle number for the porous $LiMn_2O_4$ nanosheets and the solid-state reaction synthesized $LiMn_2O_4$. Reprinted from Ref. [54] with permission from Royal Society of Chemistry.

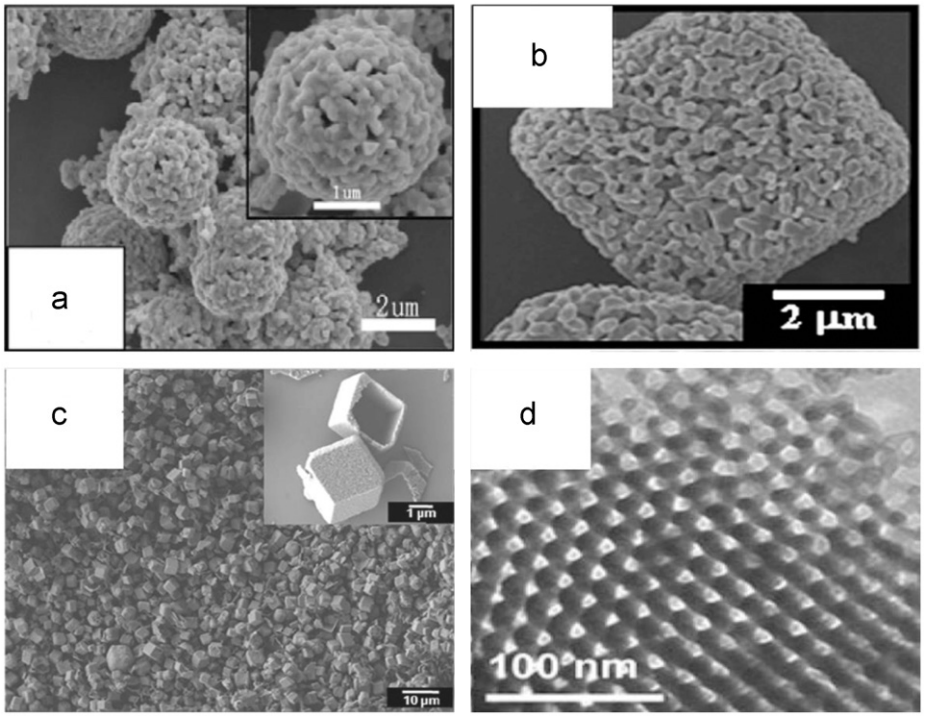

Fig. 9 (a) SEM image of $LiMn_2O_4$ porous microspheres synthesized from MnO_2 urchin-like microspheres. Reprinted from Ref. [58] with permission from Elsevier. (b) SEM image of porous spherical $LiMn_2O_4$ obtained from spherical $MnCO_3$. Reprinted from Ref. [59] with permission from Royal Society of Chemistry. (c) SEM image of hollow porous $LiMn_2O_4$ microcubes synthesized from $MnCO_3$ hollow microcubes. Reprinted from Ref. [60] with permission from John Wiley and Sons. (d) TEM image of ordered mesoporous $LiMn_2O_4$ synthesized using mesoporous silica. Reprinted from Ref. [61] with permission from John Wiley and Sons.

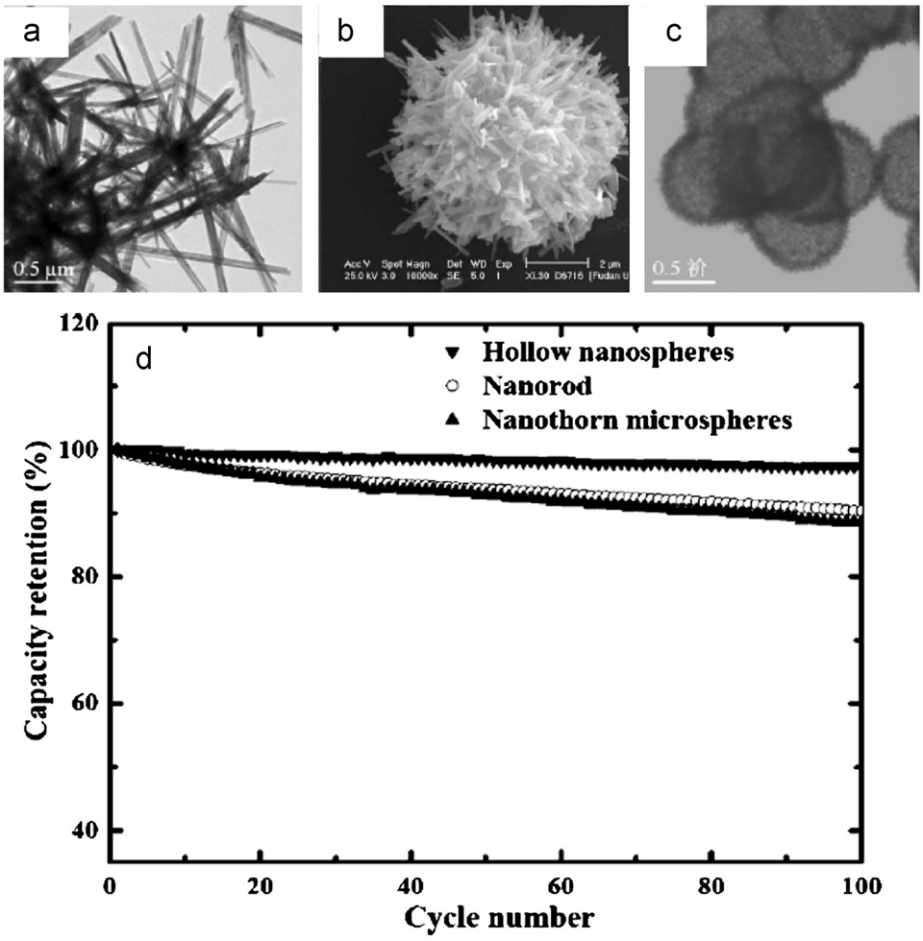

Fig. 10 (a) TEM image of $LiMn_2O_4$ nanorods. (b) SEM image of $LiMn_2O_4$ nanothorn microspheres. (c) TEM image of $LiMn_2O_4$ hollow nanospheres. (d) Cycle performance of the three different $LiMn_2O_4$ nanostructures. Reprinted from Ref. [62] with permission from American Chemical Society.

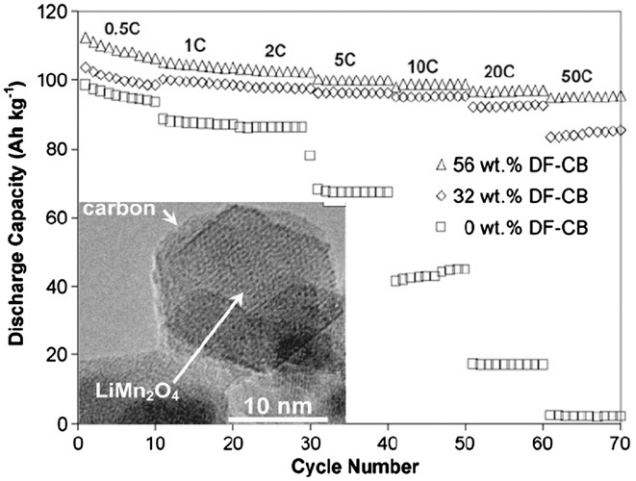

Fig. 11 Discharge capacities for electrodes with the FSP-produced $LiMn_2O_4$ nanoparticles and various co-produced carbon black contents at various C-rates between 3.5 and 4.3 V vs. Li/Li^+. Reprinted from Ref. [28] with permission from Elsevier.

vapor- and liquid-fed flame technology for flame co-synthesis of $LiMn_2O_4$/C nanocomposites. The synthesized $LiMn_2O_4$/C nanocomposites had an average $LiMn_2O_4$ particle size of 10 nm and exhibited excellent rate capability. The electrodes could retain more than 80% of their nominal discharge capacities even when cycled up to a 50 C rate (Fig. 11). However, the carbon content is more than 32 wt% in the nanocomposites, which would cause reduction in the energy density of the electrode.

Compared to other carbon nanostructures, CNT and GNS are attractive as ideal templates to construct a hybrid material with good dispersion of nanoparticles and improved electrical conductivity [69]. Liu et al. synthesized $LiMn_2O_4$/CNT nanocomposites (CNT content 10 wt%) by a sol–gel method [65]. Although $LiMn_2O_4$ nanoparticles of 20–40 nm in diameter were obtained, severe aggregation was still observed in the nanocomposites (Fig. 12a). Since a low calcination temperature (250 °C) was used for the final synthesis step, these $LiMn_2O_4$ nanoparticles were poorly crystallized, which lead to the limited capacity of about 70 mA h/g. Jia et al. reported the synthesis of $LiMn_2O_4$/CNT nanocomposites (CNT content 11 wt%) by a two-step hydrothermal method [66]. The second step of the hydrothermal treatment was performed at 180 °C for 4 days and produced highly crystallized $LiMn_2O_4$ nanoparticles of 50–100 nm in diameter (Fig. 12b). Their nanocomposites could deliver a discharge capacity of about 109 mA h/g without using any binder in the electrode. To further reduce the particle size of $LiMn_2O_4$ in the nanocomposites, Xia et al. developed a one-step hydrothermal method using alcohol as the reducing agent and successfully

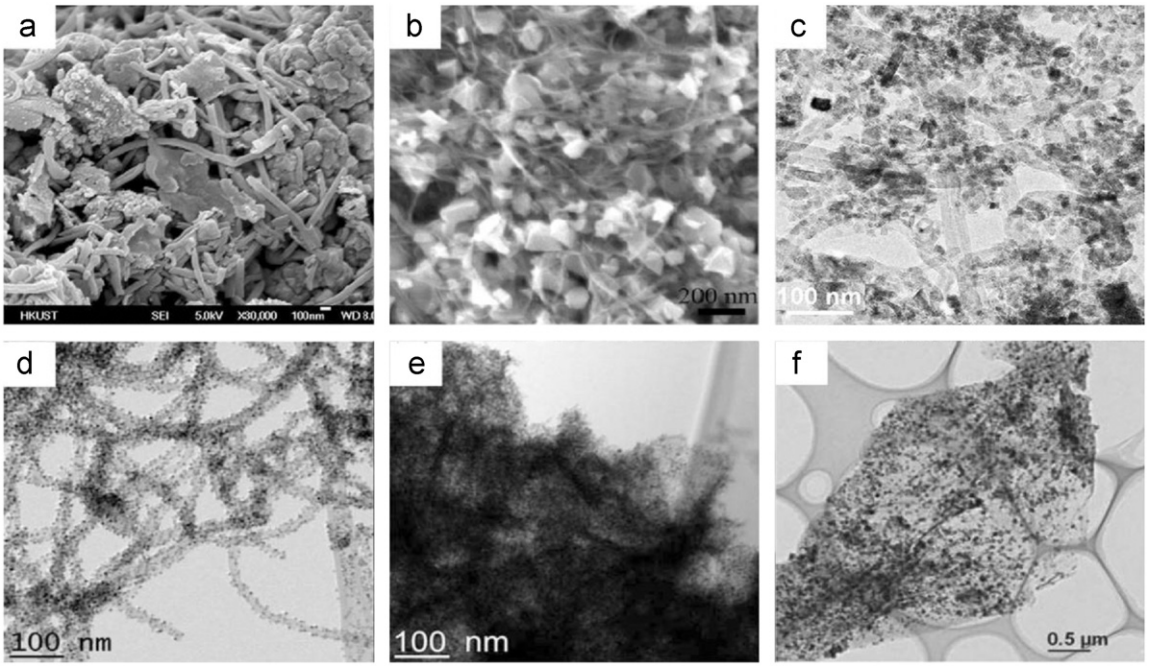

Fig. 12 (a) SEM image of $LiMn_2O_4$/CNT nanocomposites prepared by a sol-gel method. Reprinted from Ref. [65] with permission from Elsevier. (b) SEM image of $LiMn_2O_4$/CNT nanocomposites prepared by a two-step hydrothermal method. Reprinted from Ref. [66] with permission from Royal Society of Chemistry. (c) TEM image of $LiMn_2O_4$/CNT nanocomposites prepared by a one-step hydrothermal method. Reprinted from Ref. [29] with permission from Elsevier. (d) TEM image of $LiMn_2O_4$/CNT nanocomposites prepared by a solid-state reaction at 380 °C. Reprinted from Ref. [67] with permission from Royal Society of Chemistry. (e) TEM image of $LiMn_2O_4$/GNS nanocomposites prepared by a solid-state reaction at 380 °C. Reprinted from Ref. [67] with permission from Royal Society of Chemistry. (f) TEM image of $LiMn_2O_4$/GNS nanocomposites prepared by a microwave-assisted hydrothermal method. Reprinted from Ref. [68] with permission from Royal Society of Chemistry.

synthesized ultrafine $LiMn_2O_4$/CNT nanocomposites at 180 °C in 5 h [29]. In these nanocomposites, $LiMn_2O_4$ nanoparticles (10–20 nm) were well crystallized and uniformly distributed in the CNT matrix (Fig. 12c), which contributed to a high discharge capacity of about 124 mA h/g and good rate capability. However, for the $LiMn_2O_4$/CNT nanocomposites discussed above, the $LiMn_2O_4$ nanoparticles were not anchored on the surface of the CNTs but were mainly distributed in the CNT matrix. When the particle size becomes considerably small, the nanoparticle aggregation can only be partially reduced but not completely prevented by the introduction of CNTs. To overcome this problem, Zhao and Kung et al. developed a simple solid-state reaction at 380 °C and successfully prepared $LiMn_2O_4$/CNT nanocomposites with $LiMn_2O_4$ nanoparticles anchored on the CNTs [67]. As shown in Fig. 12d, for nanocomposites with a high carbon content, a monolayer or submonolayer of discrete nanoparticles (less than 10 nm in diameter) could be assembled on the CNTs. The $LiMn_2O_4$/GNS nanocomposites could also be synthesized (Fig.12e) by a similar approach [67]. These $LiMn_2O_4$/CNT (or GNS) nanocomposites exhibited very large discharge capacities that are close to the theoretical capacity of $LiMn_2O_4$ (148 mA h/g). When normalized to the $LiMn_2O_4$ content, the initial capacities of $LiMn_2O_4$/10 wt%CNT, $LiMn_2O_4$/30 wt%CNT, and $LiMn_2O_4$/6 wt%GNS nanocomposites were 159, 161, and 155 mA h/g, respectively, which exceeded the theoretical capacity (Fig. 13). The extra capacity could be attributed to the electric double-layer capacitance arising from the storage of lithium ions on the surface of CNTs and CNS [67]. Bak and Kim et al. synthesized $LiMn_2O_4$/GNS nanocomposites (carbon content 27%) using a microwave-assisted hydrothermal method at 200 °C for 30 min [68]. Their $LiMn_2O_4$ nanoparticles were evenly dispersed on the GNS template without agglomeration (Fig. 12f). The LMn_2O_4/GNS nanocomposite electrode exhibited a high discharge capacity of 137 mA h/g at 1 C rate and remarkable discharge capacities of 117 and 101 mA h/g at 50 C and 100 C rates, respectively (Fig. 14). Such high rate capability of the $LiMn_2O_4$/GNS nanocomposites was attributed to the large surface capacitive contribution from the hybrid electrode.

Recently, Lee et al. reported 3-D porous $LiMn_2O_4$/carbon nanocomposites that are nanoclusters of carbon-coated primary $LiMn_2O_4$ nanoparticles with a size of 20 nm [70]. The $LiMn_2O_4$ nanoparticles were synthesized by a low-temperature hydrothermal treatment. The carbon coating on the nanoparticles was performed by mixing the as-prepared $LiMn_2O_4$ nanoparticles with sucrose and quenching at 600 °C for 10 min. The 3-D $LiMn_2O_4$/carbon nanocomposites exhibited excellent rate capability with 83.1% capacity retained at 50 C. The excellent performance was attributed to its unique nanoarchitecture that connects every single-crystal nanoparticle electrically and ionically in parallel, thus enabling fast charge transport. Although the introduction of carbon could improve the electrochemical properties of $LiMn_2O_4$, different forms of carbon, such as carbon coating, CNT and GNS, may play different roles in the $LiMn_2O_4$/carbon nanocomposites. GNS usually exhibits larger specific surface area than CNT, which leads to better dispersity of $LiMn_2O_4$ nanoparticles in the GNS matrix. To achieve good attachment of $LiMn_2O_4$ nanoparticles on the carbon surface, acid-treated

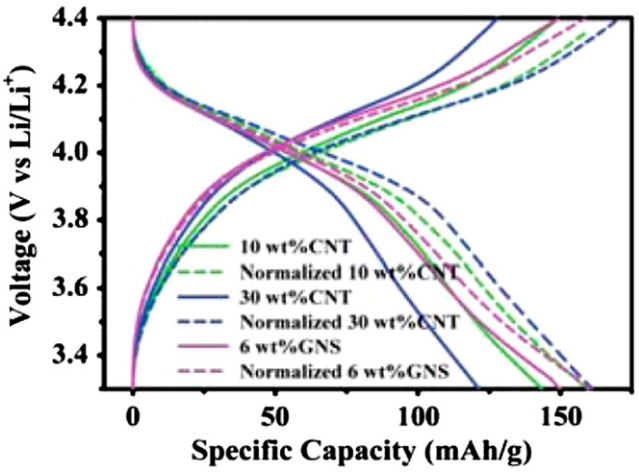

Fig. 13 First cycle charge/discharge curves of $LiMn_2O_4$/10 wt%CNT, $LiMn_2O_4$/10 wt%CNT, and $LiMn_2O_4$/10 wt%CNT in the voltage range between 3.3 and 4.4 V at 0.2 C rates. Reprinted from Ref. [67] with permission from Royal Society of Chemistry.

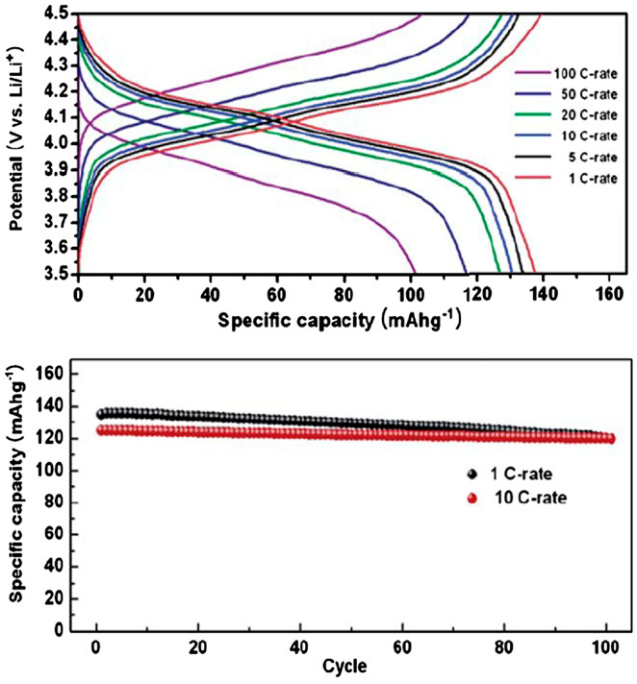

Fig. 14 Charge/discharge curves of the $LiMn_2O_4$/GNS nanocomposites electrode at various C-rates between 3.5 and 5 V vs. Li/Li^+ and cycle performance of the $LiMn_2O_4$/GNS nanocomposites electrode at different C-rates. Reprinted from Ref. [68] with permission from Royal Society of Chemistry.

CNTs and graphite oxide (GO) sheets are often used to attract metal ions. Due to the defects and functional groups of the acid-treated CNTs, the electrical conductivity of the CNTs could be decreased. GO has to be reduced to graphene to improve the electrical conductivity. Hence, the electrical conductivity of $LiMn_2O_4$/GNS nanocomposites depends on the degree of reduction of GO. While GNS and CNT cannot provide complete contact between carbon and all the surfaces of $LiMn_2O_4$ nanoparticles, a uniform carbon coating on the nanoparticles could achieve such complete contact, which makes it promising in improving the electrical conductivity of the nanocomposites. However, the electrical conductivity of coated carbon also depends on the degree of graphitization during the high-temperature annealing process. As discussed in the previous part, high-temperature processing could lead to oxygen deficiency of $LiMn_2O_4$ due to the strong reductivity of carbon. Therefore, it is still a challenge to coat a highly conductive carbon layer on the $LiMn_2O_4$ nanoparticles without changing the stoichiometry of $LiMn_2O_4$.

3. Conclusions

Nanostructured $LiMn_2O_4$ and $LiMn_2O_4$-carbon nanocomposites will play a more and more important role in developing high performance lithium-ion batteries for high power applications such as EV and HEV. The features of nanostructured $LiMn_2O_4$, such as large surface area, short diffusion paths for lithium diffusion and electron transfer, and improved structural stability against volume changes during cycling, enable the electrodes to achieve larger capacity, better rate capability and cycling stability than their bulk counterparts. However, nanoparticle aggregation and low degree of crystallinity, which can degrade their electrochemical performance, are the two common problems for the nanostructured $LiMn_2O_4$. Except for nanoparticles, most of 1-D, 2-D and 3-D $LiMn_2O_4$ nanostructures are synthesized using manganese oxides or manganese carbonates as self-templates. The incorporation of CNT or GNS in $LiMn_2O_4$ can partially solve the problem of particle aggregation and improve the electrical conductivity of the electrode, thereby improving the rate capability. However, a high content of carbon in the nanocomposites would reduce the energy density of the electrode. Hence, further optimization of the CNT and GNS contents in the nanocomposites is required. To achieve a wide range of industrial applications, the development of new synthetic routes of nanostructured $LiMn_2O_4$ and $LiMn_2O_4$/carbon nanocomposites that have simple procedure and are capable of mass production is necessary and remains a challenge.

Acknowledgements

This work was supported by National Natural Science Foundation of China (No. 51102134), Nanjing University of Science and Technology through NUST Research Funding (No. 2011ZDJH21 and AB41385), and Key Laboratory of Soft Chemistry and Functional Materials through the open fund 2012KSFM05.

References

[1] P.G. Bruce, B. Scrosati, J.-M. Tarascon, Nanomaterials for rechargeable lithium batteries, Angewandte Chemie International Edition 47 (2008) 2930–2946.
[2] Y.-G. Guo, J.-S. Hu, L.-J. Wan, Nanostructured materials for electrochemical energy conversion and storage devices, Advanced Materials 20 (2008) 2878–2887.
[3] F. Cheng, J. Liang, Z. Tao, J. Chen, Functional materials for rechargeable batteries, Advanced Materials 23 (2011) 1695–1715.
[4] D. Chen, X. Mei, G. Ji, M. Lu, J. Xie, J. Lu, J.Y. Lee, Reversible lithium-ion Storage in silver-treated nanoscale hollow porous silicon particles, Angewandte Chemie International Edition 51 (2012) 2409–2413.

[5] V. Etacheri, R. Marom, R. Elazari, G. Salitra, D. Aurbach, Challenges in the development of advanced Li-ion batteries: a review, Energy & Environmental Science 4 (2011) 3243–3262.
[6] M.S. Whittingham, Lithium batteries and cathode naterials, Chemical Reviews 104 (2004) 4271–4302.
[7] M.-K. Song, S. Park, F.M. Alamgir, J. Cho, M. Liu, Nanostructured electrodes for lithium-ion and lithium-air batteries: the latest developments, challenges, and perspectives, Materials Science and Engineering Reports 72 (2011) 203–252.
[8] H. Xia, Y.S. Meng, M.O. Lai, L. Lu, Structural and electrochemical properties of $LiNi_{0.5}Mn_{0.5}O_2$ thin-film electrodes prepared by pulsed laser deposition, Journal of The Electrochemical Society 157 (2010) A348–A354.
[9] H. Xia, L. Lu, Y.S. Meng, Growth of layered $LiNi_{0.5}Mn_{0.5}O_2$ thin films by pulsed laser deposition for application in microbatteries, Applied Physics Letters 92 (2008) 011912-3.
[10] A. Manthiram, Materials challenges and opportunities of lithium ion batteries, The Journal of Physical Chemistry Letters 2 (2011) 176–184.
[11] R. Pitchai, V. Thavasi, S.G. Mhaisalkar, S. Ramakrishna, Nanostructured cathode materials: a key for better performance in Li-ion batteries, Journal of Materials Chemistry 21 (2011) 11040–11051.
[12] M.M. Thackeray, Manganese oxides for lithium batteries, Progress in Solid State Chemistry 25 (1997) 1–71.
[13] M.M. Thackeray, Y. ShaoHorn, A.J. Kahaian, K.D. Kepler, E. Skinner, J.T. Vaughey, S.A. Hackney, Structural fatigue in spinel electrodes in high voltage (4 V) $Li/Li_xMn_2O_4$ Cells, Electrochemical and Solid-State Letters 1 (1998) 7–9.
[14] D. Guan, J.A. Jeevarajan, Y. Wang, Enhanced cycleability of $LiMn_2O_4$ cathodes by atomic layer deposition of nanosized-thin Al_2O_3 coatings, Nanoscale 3 (2011) 1465–1469.
[15] Y. Xia, M. Yoshio, An investigation of lithium ion insertion into spinel structure LiMnO compounds, Journal of The Electrochemical Society 143 (1996) 825–833.
[16] H. Huang, C.A. Vincent, P.G. Bruce, Correlating capacity loss of stoichiometric and nonstoichiometric lithium manganese oxide spinel electrodes with their structural integrity, Journal of The Electrochemical Society 146 (1999) 3649–3654.
[17] Y. Shin, A. Manthiram, Microstrain and capacity fade in spinel manganese oxides, Electrochemical and Solid-State Letters 5 (2002) A55–A58.
[18] M. Okubo, Y. Mizuno, H. Yamada, J. Kim, E. Hosono, H. Zhou, T. Kudo, I. Honma, Fast Li-ion insertion into nanosized $LiMn_2O_4$ without domain boundaries, ACS Nano 4 (2010) 741–752.
[19] H. Xia, H. Wang, W. Xiao, L. Lu, M.O. Lai, Properties of $LiNi_{1/3}Co_{1/3}Mn_{1/3}O_2$ cathode material synthesized by a modified Pechini method for high-power lithium-ion batteries, Journal of Alloys and Compounds 480 (2009) 696–701.
[20] H. Xia, M. Lai, L. Lu, Nanoflaky MnO_2/carbon nanotube nanocomposites as anode materials for lithium-ion batteries, Journal of Materials Chemistry 20 (2010) 6896–6902.
[21] W. Tang, L.L. Liu, S. Tian, L. Li, L.L. Li, Y.B. Yue, Y. Bai, Y.P. Wu, K. Zhu, R. Holze, $LiMn_2O_4$ nanorods as a super-fast cathode material for aqueous rechargeable lithium batteries, Electrochemistry Communications 13 (2011) 1159–1162.
[22] T.J. Patey, R. Buchel, M. Nakayama, P. Novak, Electrochemistry of $LiMn_2O_4$ nanoparticles made by flame spray pyrolysis, Physical Chemistry Chemical Physics 11 (2009) 3756–3761.
[23] Y. Yang, C. Xie, R. Ruffo, H. Peng, D.K. Kim, Y. Cui, Single nanorod devices for battery diagnostics: a case study on $LiMn_2O_4$, Nano Letters 9 (2009) 4109–4114.
[24] E. Hosono, T. Kudo, I. Honma, H. Matsuda, H. Zhou, Synthesis of single crystalline spinel $LiMn_2O_4$ nanowires for a lithium ion battery with high power density, Nano Letters 9 (2009) 1045–1051.
[25] Y.-k. Zhou, C.-m. Shen, J. Huang, H.-l. Li, Synthesis of high-ordered $LiMn_2O_4$ nanowire arrays by AAO template and its structural properties, Materials Science and Engineering B 95 (2002) 77–82.
[26] Y.-L. Ding, J. Xie, G.-S. Cao, T.-J. Zhu, H.-M. Yu, X.-B. Zhao, Single-crystalline $LiMn_2O_4$ nanotubes synthesized via template-engaged reaction as cathodes for high-power lithium ion batteries, Advanced Functional Materials 21 (2011) 348–355.
[27] X. Li, F. Cheng, B. Guo, J. Chen, Template-synthesized $LiCoO_2$, $LiMn_2O_4$, and $LiNi_{0.8}Co_{0.2}O_2$ nanotubes as the cathode materials of lithium ion batteries, The Journal of Physical Chemistry B 109 (2005) 14017–14024.
[28] T.J. Patey, R. Büchel, S.H. Ng, F. Krumeich, S.E. Pratsinis, P. Novák, Flame co-synthesis of $LiMn_2O_4$ and carbon nanocomposites for high power batteries, Journal of Power Sources 189 (2009) 149–154.
[29] H. Xia, K.R. Ragavendran, J. Xie, L. Lu, Ultrafine $LiMn_2O_4$/carbon nanotube nanocomposite with excellent rate capability and cycling stability for lithium-ion batteries, Journal of Power Sources 212 (2012) 28–34.
[30] J.F. von Bülow, H.-L. Zhang, D.E. Morse, Hydrothermal realization of high-power nanocomposite cathodes for lithium ion batteries, Advanced Energy Materials 2 (2012) 309–315.
[31] S.Y. Han, I.Y. Kim, K.Y. Jo, S.-J. Hwang, Solvothermal-assisted hybridization between reduced graphene oxide and lithium metal oxides: a facile route to graphene-based composite materials, The Journal of Physical Chemistry C 116 (2012) 7269–7279.
[32] Y. Tong, M. Shao, Y. Ni, G. Qian, Y. Ye, P. Zhang, Low temperature route to nanocrystalline $LiMn_2O_4$ spinel, Materials Letters 60 (2006) 2578–2581.
[33] S. Vivekanandhan, M. Venkateswarlu, N. Satyanarayana, P. Suresh, D.H. Nagaraju, N. Munichandraiah, Effect of calcining temperature on the electrochemical performance of nanocrystalline $LiMn_2O_4$ powders prepared by polyethylene glycol (PEG-400) assisted Pechini process, Materials Letters 60 (2006) 3212–3216.
[34] X. Wang, X. Chen, L. Gao, H. Zheng, M. Ji, T. Shen, Z. Zhang, Citric acid-assisted sol–gel synthesis of nanocrystalline $LiMn_2O_4$ spinel as cathode material, Journal of Crystal Growth 256 (2003) 123–127.
[35] C.-Z. Lu, G.T.-K. Fey, Nanocrystalline and long cycling $LiMn_2O_4$ cathode material derived by a solution combustion method for lithium ion batteries, Journal of Physics and Chemistry of Solids 67 (2006) 756–761.
[36] S.-H. Park, S.-T. Myung, S.-W. Oh, C.S. Yoon, Y.-K. Sun, Ultrasonic spray pyrolysis of nano crystalline spinel $LiMn_2O_4$ showing good cycling performance in the 3 V range, Electrochimica Acta 51 (2006) 4089–4095.
[37] K. Sathiyaraj, G.D. Bhuvaneswari, N. Kalaiselvi, A.J. Peter, H_2O_2-aided one-pot hydrothermal synthesis of nanocrystalline $LiMn_2O_4$ cathode for lithium batteries, IEEE Transactions on Nanotechnology 11 (2012) 314–320.
[38] Y. Chen, K. Xie, Y. Pan, C. Zheng, Nano-sized $LiMn_2O_4$ spinel cathode materials exhibiting high rate discharge capability for lithium-ion batteries, Journal of Power Sources 196 (2011) 6493–6497.
[39] P. Ragupathy, H.N. Vasan, N. Munichandraiah, Microwave driven hydrothermal synthesis of $LiMn_2O_4$ nanoparticles as cathode material for Li-ion batteries, Materials Chemistry and Physics 124 (2010) 870–875.
[40] R. Thirunakaran, A. Sivashanmugam, S. Gopukumar, C.W. Dunnill, D.H. Gregory, Electrochemical behaviour of nano-sized spinel $LiMn_2O_4$ and $LiAl_xMn_{2-x}O_4$ (x = Al: 0.00–0.40) synthesized via fumaric acid-assisted sol–gel synthesis for use in lithium rechargeable batteries, Journal of Physics and Chemistry of Solids 69 (2008) 2082–2090.
[41] W. Tang, X.J. Wang, Y.Y. Hou, L.L. Li, H. Sun, Y.S. Zhu, Y. Bai, Y.P. Wu, K. Zhu, T. van Ree, Nano $LiMn_2O_4$ as cathode material of high rate capability for lithium ion batteries, Journal of Power Sources 198 (2012) 308–311.
[42] J.H. Yi, J.H. Kim, H.Y. Koo, Y.N. Ko, Y.C. Kang, J.-H. Lee, Nanosized $LiMn_2O_4$ powders prepared by flame spray pyrolysis from aqueous solution, Journal of Power Sources 196 (2011) 2858–2862.
[43] K.M. Shaju, P.G. Bruce, A stoichiometric nano-$LiMn_2O_4$ spinel electrode exhibiting high power and stable cycling, Chemistry of Materials 20 (2008) 5557–5562.

[44] Y. Chen, K. Xie, Y. Pan, C. Zheng, Effect of calcination temperature on the electrochemical performance of nanocrystalline $LiMn_2O_4$ prepared by a modified resorcinol–formaldehyde route, Solid State Ionics 181 (2010) 1445–1450.
[45] W. Tang, S. Tian, L.L. Liu, L. Li, H.P. Zhang, Y.B. Yue, Y. Bai, Y.P. Wu, K. Zhu, Nanochain LiMn2O4 as ultra-fast cathode material for aqueous rechargeable lithium batteries, Electrochemistry Communications 13 (2011) 205–208.
[46] C.H. Jiang, S.X. Dou, H.K. Liu, M. Ichihara, H.S. Zhou, Synthesis of spinel $LiMn_2O_4$ nanoparticles through one-step hydrothermal reaction, Journal of Power Sources 172 (2007) 410–415.
[47] H.M. Wu, J.P. Tu, Y.F. Yuan, X.T. Chen, J.Y. Xiang, X.B. Zhao, G.S. Cao, One-step synthesis $LiMn_2O_4$ cathode by a hydrothermal method, Journal of Power Sources 161 (2006) 1260–1263.
[48] B.J. Liddle, S.M. Collins, B.M. Bartlett, A new one-pot hydrothermal synthesis and electrochemical characterization of $Li_{1+x}Mn_{2-y}O_4$ spinel structured compounds, Energy & Environmental Science 3 (2010) 1339–1346.
[49] X. Hao, O. Gourdon, B.J. Liddle, B.M. Bartlett, Improved electrode kinetics in lithium manganospinel nanoparticles synthesized by hydrothermal methods: identifying and eliminating oxygen vacancies, Journal of Materials Chemistry 22 (2012) 1578–1591.
[50] D.K. Kim, P. Muralidharan, H.-W. Lee, R. Ruffo, Y. Yang, C.K. Chan, H. Peng, R.A. Huggins, Y. Cui, Spinel $LiMn_2O_4$ nanorods as lithium ion battery cathodes, Nano Letters 8 (2008) 3948–3952.
[51] H.-W. Lee, P. Muralidharan, R. Ruffo, C.M. Mari, Y. Cui, D.K. Kim, Ultrathin spinel $LiMn_2O_4$ nanowires as high power cathode materials for Li-ion batteries, Nano Letters 10 (2010) 3852–3856.
[52] C. Wang, Y. Zhou, M. Ge, X. Xu, Z. Zhang, J.Z. Jiang, Large-scale synthesis of SnO_2 nanosheets with high lithium storage capacity, Journal of the American Chemical Society 132 (2009) 46–47.
[53] N. Wang, Y. Sakai, K. Ebina, T. Takada, Sasaki, Inorganic multilayer films of manganese oxide nanosheets and aluminum polyoxocations: fabrication, structure, and electrochemical behavior, Chemistry of Materials 17 (2005) 1352–1357.
[54] W. Sun, F. Cao, Y. Liu, X. Zhao, X.G. Liu, J. Yuan, Nanoporous $LiMn_2O_4$ nanosheets with exposed {1 1 1} facets as cathodes for highly reversible lithium-ion batteries, Journal of Materials Chemistry (in press).
[55] J.M. Kim, G. Lee, B.H. Kim, Y.S. Huh, G.-W. Lee, H.J. Kim, Ultrasound-assisted synthesis of Li-rich mesoporous $LiMn_2O_4$ nanospheres for enhancing the electrochemical performance in Li-ion secondary batteries, Ultrasonics Sonochemistry 19 (2012) 627–631.
[56] Q. Qu, L. Fu, X. Zhan, D. Samuelis, J. Maier, L. Li, S. Tian, Z. Li, Y. Wu, Porous $LiMn_2O_4$ as cathode material with high power and excellent cycling for aqueous rechargeable lithium batteries, Energy & Environmental Science 4 (2011) 3985–3990.
[57] F. Cheng, H. Wang, Z. Zhu, Y. Wang, T. Zhang, Z. Tao, J. Chen, Porous $LiMn_2O_4$ nanorods with durable high-rate capability for rechargeable Li-ion batteries, Energy & Environmental Science 4 (2011) 3668–3675.
[58] L.J. Xi, H.-E. Wang, Z.G. Lu, S.L. Yang, R.G. Ma, J.Q. Deng, C.Y. Chung, Facile synthesis of porous $LiMn_2O_4$ spheres as positive electrode for high-power lithium ion batteries, Journal of Power Sources 198 (2012) 251–257.
[59] H. Uchiyama, E. Hosono, H. Zhou, H. Imai, Three-dimensional architectures of spinel-type $LiMn_2O_4$ prepared from biomimetic porous carbonates and their application to a cathode for lithium-ion batteries, Journal of Materials Chemistry 19 (2009) 4012–4016.
[60] Y. Wu, Z. Wen, H. Feng, J. Li, Hollow porous $LiMn_2O_4$ microcubes as rechargeable lithium battery cathode with high electrochemical performance, Small 8 (2012) 858–862.
[61] F. Jiao, J. Bao, A.H. Hill, P.G. Bruce, Synthesis of ordered mesoporous Li–Mn–O spinel as a positive electrode for rechargeable lithium batteries, Angewandte Chemie International Edition 47 (2008) 9711–9716.
[62] J.-Y. Luo, H.-M. Xiong, Y.-Y. Xia, $LiMn_2O_4$ nanorods, nanothorn microspheres, and hollow nanospheres as enhanced cathode materials of lithium ion battery, The Journal of Physical Chemistry C 112 (2008) 12051–12057.
[63] J. Luo, L. Cheng, Y. Xia, $LiMn_2O_4$ hollow nanosphere electrode material with excellent cycling reversibility and rate capability, Electrochemistry Communications 9 (2007) 1404–1409.
[64] H. Yue, X. Huang, D. Lv, Y. Yang, Hydrothermal synthesis of $LiMn_2O_4$/C composite as a cathode for rechargeable lithium-ion battery with excellent rate capability, Electrochimica Acta 54 (2009) 5363–5367.
[65] X.-M. Liu, Z.-D. Huang, S. Oh, P.-C. Ma, P.C.H. Chan, G.K. Vedam, K. Kang, J.-K. Kim, Sol–gel synthesis of multiwalled carbon nanotube–$LiMn_2O_4$ nanocomposites as cathode materials for Li-ion batteries, Journal of Power Sources 195 (2010) 4290–4296.
[66] X. Jia, C. Yan, Z. Chen, R. Wang, Q. Zhang, L. Guo, F. Wei, Y. Lu, Direct growth of flexible $LiMn_2O_4$/CNT lithium-ion cathodes, Chemical Communications 47 (2011) 9669–9671.
[67] X. Zhao, C.M. Hayner, H.H. Kung, Self-assembled lithium manganese oxide nanoparticles on carbon nanotube or graphene as high-performance cathode material for lithium-ion batteries, Journal of Materials Chemistry 21 (2011) 17297–17303.
[68] S.-M. Bak, K.-W. Nam, C.-W. Lee, K.-H. Kim, H.-C. Jung, X.-Q. Yang, K.-B. Kim, Spinel $LiMn_2O_4$/reduced graphene oxide hybrid for high rate lithium ion batteries, Journal of Materials Chemistry 21 (2011) 17309–17315.
[69] Y. Fu, Y. Wan, H. Xia, X. Wang, Nickel ferrite–graphene heteroarchitectures: toward high-performance anode materials for lithium-ion batteries, Journal of Power Sources 213 (2012) 338–342.
[70] S. Lee, Y. Cho, H.-K. Song, K.T. Lee, J. Cho, Carbon-coated single-crystal $LiMn_2O_4$ nanoparticle clusters as cathode material for high-energy and high-power lithium-ion batteries, Angewandte Chemie International Edition 51 (2012) 8748–8752.

Jianping Xie received his B.S. and M.S. in Chemical Engineering from Tsinghua University of China. He graduated with Ph.D. from the Singapore-MIT Alliance (SMA) program. He joined National University of Singapore as an Assistant Professor in 2010. His current research interests lie in the interfacing of nanotechnology and biotechnology with focus on developing green chemistry for the synthesis of functional inorganic nanomaterials and exploring their biomedical and energy applications. He has published more than 30 papers in journals such as Nature Communications, JACS, ACIE, ACS Nano and Small; and has more than 1000 citations. Email: chexiej@nus.edu.sg; website: http://cheed.nus.edu.sg/~chexiej/index.html.

Hui Xia received his B.E. and M.E. in Materials Science and Engineering from University of Science and Technology Beijing. He obtained his Ph.D. degree in Advanced Materials for Micro- and Nano-Systems from Singapore-MIT Alliance, National University of Singapore, in 2008. He is now an Associate Professor in School of Materials Science and Engineering, Nanjing University of Science and Technology. His research interests include electrode materials for lithium-ion batteries and supercapacitors, fabrication of all-solid-state thin film microbatteries, and gas sensors. He has published over 50 papers in international journals with more than 700 citations.